Journal of Power Sources 243 (2013) 203–210

Contents lists available at SciVerse ScienceDirect

Journal of Power Sources

journal homepage: www.elsevier.com/locate/jpowsour

Molybdenum dioxide-based anode for solid oxide fuel cell applications

Byeong Wan Kwon [a], Caleb Ellefson [b], Joe Breit [c], Jinsoo Kim [d], M. Grant Norton [b,**], Su Ha [a,d,*]

[a] Voiland School of Chemical Engineering and Bioengineering, Washington State University, P.O. Box 642710, Pullman, WA 99164-2710, USA
[b] School of Mechanical and Materials Engineering, Washington State University, P.O. Box 642920, Pullman, WA 99164-2920, USA
[c] System Concept Center, Boeing Commercial Airplanes, 6600 Merrill Creek Pkwy., Everett, WA 98203, USA
[d] Department of Chemical Engineering, Kyung Hee University, 1 Seocheon-dong Giheung-gu, Yongin, Gyeonggi-do 449-701, Republic of Korea

HIGHLIGHTS

- A novel MoO_2-based anode for liquid-fueled SOFC application was developed.
- The MoO_2-based SOFC was successfully operated using both *n*-dodecane and biodiesel.
- The MoO_2-based SOFC at 850 °C showed a maximum power density of 2500 mW cm^{-2}.
- The MoO_2-based anode displayed a stable performance over 24 h.

GRAPHICAL ABSTRACT

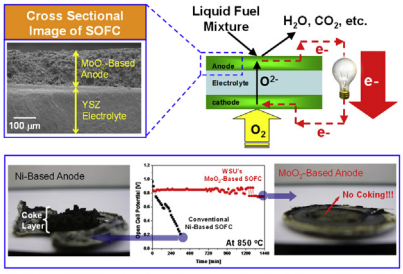

MoO_2-based SOFC using a fuel mixture consisting of n-dodecane, CO_2, and air

ARTICLE INFO

Article history:
Received 8 November 2012
Received in revised form
24 May 2013
Accepted 25 May 2013
Available online 5 June 2013

Keywords:
Solid oxide fuel cells
Molybdenum dioxide
Anode
n-Dodecane
Biodiesel

ABSTRACT

The present paper describes the fabrication and performance of a molybdenum dioxide (MoO_2)-based anode for liquid hydrocarbon/oxygenated hydrocarbon-fueled solid oxide fuel cells (SOFCs). These fuel cells first internally reform the complex liquid fuel into carbon fragments and hydrogen, which are then electrochemically oxidized to produce electrical energy without external fuel processors. The MoO_2-based anode was fabricated on to an yttria-stabilized zirconia (YSZ) electrolyte via combined electrostatic spray deposition (ESD) and direct painting methods. The cell performance was measured by directly feeding liquid fuels such as *n*-dodecane (i.e., a model diesel/kerosene fuel) or biodiesel (i.e., a future biomass-based liquid fuel) to the MoO_2-based anode at 850 °C. The maximum initial power densities obtained from our MoO_2-based SOFC were 34 mW cm^{-2} and 45 mW cm^{-2} using *n*-dodecane and biodiesel, respectively. The initial power density of the MoO_2-based SOFC was improved up to 2500 mW cm^{-2} by optimizing the porosity of the MoO_2-based anode. To test the long-term stability of the MoO_2-based anode SOFC against coking, *n*-dodecane was continuously fed into the cell for 24 h at the open circuit voltage (OCV). During long-term testing, voltage–current density (*V*–*I*) plots were periodically obtained and they showed no significant changes over the operation time. Microstructural examination of the tested cells indicated that the MoO_2-based anode displayed negligible coke formation, which explains its stability. On the other hand, SOFCs with conventional nickel (Ni)-based anodes under the same operating conditions showed a significant amount of coke formation on the metal surface, which led to a rapid drop in cell performance. Hence, the present work demonstrates that MoO_2-based

* Corresponding author. Voiland School of Chemical Engineering and Bioengineering, Washington State University, P.O. Box 642710, Pullman, WA 99164-2710, USA. Tel.: +1 509 335 3786; fax: +1 509 335 4806.
** Corresponding author. Tel.: +1 509 335 6617.
E-mail addresses: mg_norton@wsu.edu (M. Grant Norton), suha@wsu.edu (S. Ha).

0378-7753/$ – see front matter Published by Elsevier B.V.
http://dx.doi.org/10.1016/j.jpowsour.2013.05.133

anodes exhibit outstanding tolerance to coke formation. This result opens up the opportunity for more efficiently generating electrical energy from both existing transportation and next generation biomass-derived liquid fuels using liquid hydrocarbon/oxygenated hydrocarbon-fueled SOFCs.

Published by Elsevier B.V.

1. Introduction

A fuel cell is an energy conversion device that enables efficient and clean conversion of chemical energy in fuels directly into electrical energy. There are several different types of fuel cells including: polymer electrolyte membrane fuel cells (PEMFCs), alkaline fuel cells (AFCs), phosphoric acid fuel cells (PAFCs), solid oxide fuel cells (SOFCs), and molten carbonate fuel cell (MCFCs) [e.g., 1–3]. Among these types, SOFCs have attracted a great deal of interest due to their high efficiency, fuel flexibility, high reliability, and low material cost. SOFCs can be operated with a variety of liquid fuels, such as conventional liquid transportation fuels and next generation liquid bio-fuels, by using external reforming systems or directly feeding these fuels to the SOFC anode [2–4]. A significant advantage of liquid hydrocarbon/oxygenated hydrocarbon fuel SOFCs, where the fuel is directly fed to the anode, is the simplicity afforded by not having to externally reform the fuel. Nickel (Ni)-based anodes are commonly used for SOFCs. However, the major disadvantages of Ni-based anodes are severe coke formation and low sulfur tolerance. Excessive coke formation on the anode leads to rapid deactivation of the cell by physically blocking the catalyst surface from the reactants. Similar to the problem with coking, sulfur compounds present in fossil-based liquid fuels can quickly deactivate the cell by forming nickel sulfide on the surface [3–12].

A number of groups have studied alternate anode materials in attempts to overcome the limitation of Ni-based anodes when liquid fuels are used directly [e.g., 13–16]. The studies conducted in this area have focused on low-cost materials with key features such as high electronic and ionic conductivities, high reforming activity, resistance to coking, and sulfur tolerance. Based on our previous researches, MoO_2 has been identified as a potential anode material that possesses all of these characteristics. Unlike previously studied transition metal oxides (e.g., CeO_2) in SOFC applications, MoO_2 possesses a significant metallic component to its interatomic bonding and has an electronic conductivity comparable to that of many metals [17,18] and highly conductive oxides such as ReO_3 [19]. The high electronic conductivity is associated with a relatively high density of states in the valence band [18]. Due to this unique combination of properties, MoO_2 has been found to display a high catalytic activity for the partial oxidation of various hydrocarbons including gasoline and Jet-A fuel. The catalytic activity has been explained in terms of the Mars-van Krevelen reaction mechanism [20–22]. Additionally, the capability of MoO_2 to selectively transfer lattice oxygen to the hydrocarbon fuel reduces the amount of carbon accumulated on the catalyst surface and minimizes coke formation during the reformation of logistics fuels [21]. For example, MoO_2 can actively catalyze the partial oxidation of Jet-A fuel over a 24 h period without showing any significant deactivation due to coking or sulfur poisoning [20]. The outstanding sulfur tolerance of MoO_2 was also demonstrated by our recent studies [e.g., 23]. Additionally, MoO_2 is much cheaper than noble metals such as Pt, which is commonly used as a catalyst in low temperature PEMFCs.

Some groups have studied Mo-based materials, including $SrMoO_4$, $Sr_2MgMoO_{6-\delta}$, and $Ho_2MoO_{6-\delta}$, as alternative anode materials for SOFC applications [24–27]. In these previous studies, MoO_x was used as a redox center where its oxidation state could change anywhere between 4+ and 6+. In this capacity, MoO_x acted as a catalyst site with a limited ability to conduct both electrons and ions. To provide the needed mixed oxide-ion/electron conductivity for the SOFC anode, MoO_x was incorporated into a perovskite structure by mixing it with other metals. However, instead of using these complex multi-cation perovskite materials single phase MoO_2 with a distorted rutile structure could be used as the sole anode material and act as the catalyst site and an ion and electron conductor.

The aim of this research was to investigate the initial performance and long-term stability of MoO_2-based SOFCs operating at 850 °C under the liquid hydrocarbon/oxygenated hydrocarbon-fueled SOFC mode. The results were compared with commercial Ni-based SOFCs operated under identical conditions. The tested cells were characterized using various analytical techniques including scanning electron microscopy (SEM) with energy dispersive X-ray analysis (EDX) and X-ray diffraction (XRD).

2. Experimental

Both commercial Ni-based SOFCs and commercial single electrode cells (i.e., YSZ electrolyte with Sr-doped $LaMnO_3$ (LSM) cathode only) were purchased from Fuel Cell Materials (Lewis Center, OH). The YSZ thickness for both commercial cells was 150 μm. The thickness of the LSM cathode and the Ni-based anode were 50 μm. The diameter of each electrode was 12.5 mm, while the electrolyte diameter was 25 mm. Both nanoparticle MoO_2 and commercially available MoO_2 were used to fabricate the MoO_2-based anode via the combined electrostatic spray deposition (ESD) and painting methods. MoO_2 nanoparticles were prepared by reduction of molybdenum trioxide (MoO_3) powder in a 1:3 volume ratio of ethylene glycol to nano-pure water [28]. Commercial MoO_2 was purchased from Alfa Aesar (Ward Hill, MA). Ethylene glycol and polyvinyl alcohol (PVA) both from Sigma Aldrich (Milwaukee, WI) were used as a precursor solvent and binder/pore former, respectively, for the ESD step. The *n*-dodecane was purchased from Alfa Aesar(Ward Hill, MA) and used as a surrogate for Jet-A fuel. Canola biodiesel was purchased from Imperium Renewables (Seattle, WA). It mainly consists of methyl oleate with a chemical formula of $C_{19}H_{36}O_2$.

A quantity of 10 mg of MoO_2 nanoparticles was dissolved in a 1:1 volume ratio of ethylene glycol to nano-pure water. This MoO_2 precursor was applied over the YSZ electrolyte surface of a commercial single electrode cell to form a thin MoO_2 seed-layer via the ESD method (see Fig. 1). ESD has several advantages over conventional spray techniques, including good film adhesion to the substrate, high material deposition efficiency, and prevention of droplets from reagglomeration after atomization [29–31]. In order to produce a uniform and thin MoO_2 seed-layer, ESD requires the most stable configuration known as the con-jet spraying mode, which is achieved using the following deposition parameters: substrate temperature 300 °C; flow rate of MoO_2 precursor solution 1 ml h^{-1}; nozzle-to-substrate distance 7 cm; applied voltage 10 kV; and precursor deposition time 1 h. For the con-jet spraying mode, the liquid (i.e., the MoO_2 precursor solution) meniscus at the tip of the needle assumes a conical shape under the applied electric field, with a thin jet emerging from the cone tip. This jet breaks up further downstream into a spray of fine, charged droplets [32]. Once a uniform and thin MoO_2 seed-layer has formed on the YSZ

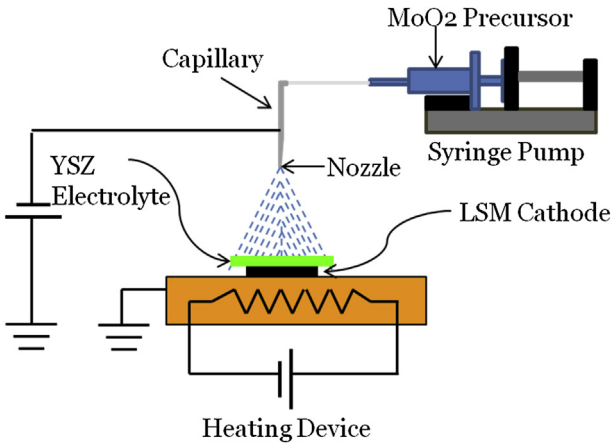

Fig. 1. Schematic of the electrostatic spray deposition (ESD) setup.

surface, a layer of MoO_2 catalyst ink is painted over this seed-layer to form the MoO_2-based anode. The MoO_2 catalyst ink was prepared by mixing commercial MoO_2 in a 1:60 weight ratio of nano-pure water to PVA binder. The resulting MoO_2-based anode does not need presintering, because it is sintered in-situ during cell operation.

Two silver wires were attached to each side of the anode and cathode for the current and voltage measurements. The anode testing compartment, shown in Fig. 2, comprises two co-axial quartz tubes. The fuel was introduced into the inner tube, and the outer tube served as an exhaust line. The assembled fuel cell was placed into a testing station that has two furnaces. The lower furnace was used to vaporize the fuel at 350 °C while the upper furnace was used to heat the entire fuel cell to 850 °C.

Air was allowed to flow through the insulation on the upper furnace into the cathode via natural convection, and it was used as the source of reducing agent for the cathode. At the anode, the fuel mixture consisted of *n*-dodecane, air, and CO_2, in the following molar ratios: 6.32:31.03:62.65. Since the fuel cell efficiency decreases as the air content increases in the fuel mixture, our fuel composition was chosen such that it contains the minimum amount of air required to stabilize the MoO_2 phase [22]. If the fuel mixture contains too little air, the MoO_2 phase will transform into Mo_2C. On the other hand, if it contains too much air, the MoO_2 phase will transform into the MoO_3 phase. Both Mo_2C and MoO_3 cannot conduct lattice oxygen, thus they will deactivate the anode performance. Furthermore, MoO_3 will sublime at the cell operating temperature of 850 °C. This fuel composition also prevented carbon deposition along the fuel lines during the cell operation.

Commercial Ni-based SOFCs were tested using similar operating conditions. Before testing commercial Ni-based SOFCs, the Ni-based anode was completely reduced in flowing H_2 at 850 °C. In order to investigate the fuel flexibility of the MoO_2-based SOFC, canola biodiesel was also used as a fuel at the following molar ratios of biodiesel, air, and CO_2 mixture: 10:30:60.

After operating both MoO_2-based and Ni-based SOFCs, the anodes were analyzed to determine the degree of coke formation using SEM (FEI Sirion operated at 15 kV) with EDX and XRD (Philips diffractometer using Co Kα radiation with an iron filter).

3. Results and discussion

Fig. 3 shows SEM cross-sectional images of the YSZ electrolyte, MoO_2 seed-layer, and MoO_2 painted layer on commercial single electrode cells. As shown in Fig. 3(c), the combined ESD and

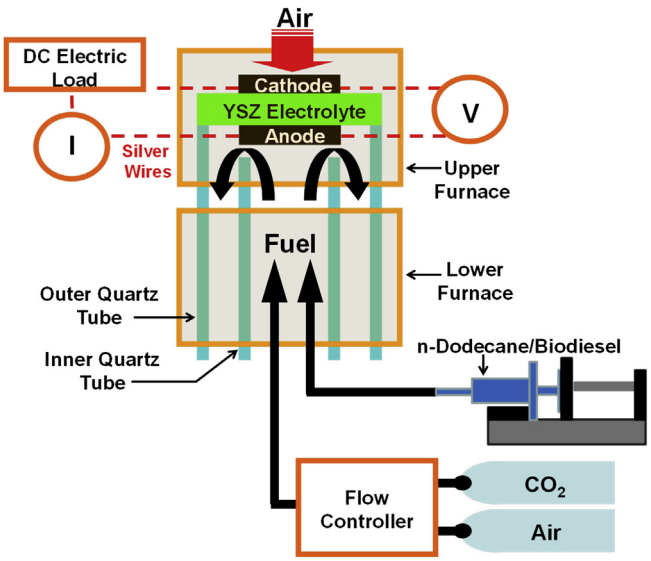

Fig. 2. Schematic view of fuel cell test station.

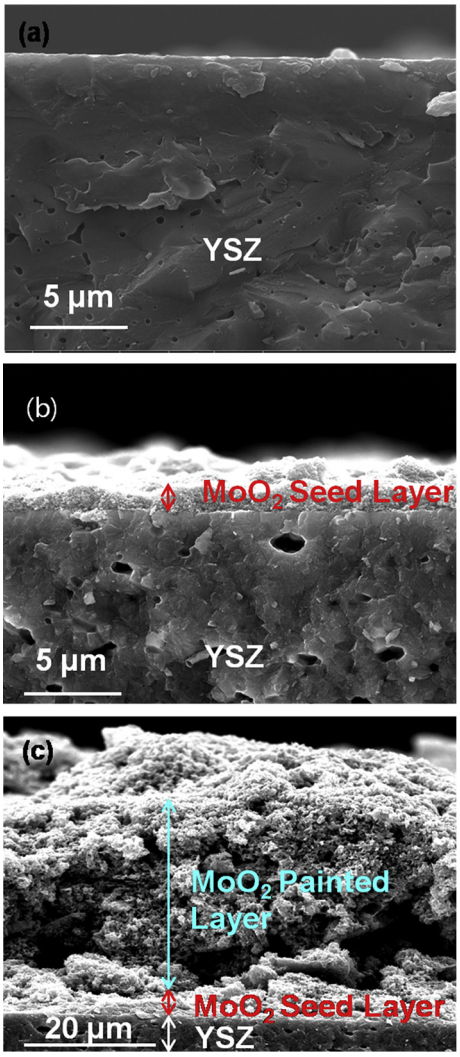

Fig. 3. SEM cross-sectional images: (a) YSZ electrolyte; (b) MoO_2 films deposited on YSZ substrate using ESD (thickness of the film ~1.5 μm); (c) MoO_2 film painted on MoO_2 seed-layer (thickness ~40 μm).

painting methods led to a porous MoO_2-based anode over the YSZ substrate. In our anode fabrication process, the ESD method allows us to make a very thin MoO_2 seed-layer (see Fig. 3(b)). At a substrate temperature of 300 °C during the EDS method, considerable evaporation of the MoO_2 precursor solution occurs before the droplets land on the YSZ substrate. As a result, the nearly dry droplets rapidly dehydrate upon landing on the YSZ surface to form fine particles. The agglomeration of these fine particles culminated in a thin film with a cauliflower-like morphology, which is strongly adherent to the YSZ substrate [33]. Thus, forming the MoO_2 seed-layer via the ESD method is a critical step to fabricate physically stable and high performing MoO_2-based anodes [34,35].

This seed-layer provides good adhesion to the YSZ, but itself is too thin to work as the anode and to provide a high cell performance. To increase the active MoO_2 anode volume, we painted additional MoO_2 layers over the seed-layer using the MoO_2 catalyst ink. When the MoO_2 catalyst ink was painted directly on the YSZ substrate without the seed-layer, the MoO_2-based anode easily detached from the YSZ electrolyte during cell operation. In general, SOFC anodes are required to go through sintering steps that increase the density of the layers and consolidate them to achieve good contact and bonding between particles [4]. However, the MoO_2-based anode does not need this presintering processes, because it can be sintered in-situ during the cell operation.

Fig. 4(a) shows voltage–current density (*V–I*) plots of a Ni-based SOFC operated at 850 °C using *n*-dodecane as the fuel. The *V–I* plots were taken every hour to investigate how the cell performance changed with time. Between *V–I* plots, the cell was operated at its open circuit voltage (OCV) condition. In the conventional Ni-based anode, fuel oxidation occurs at triple-phase boundary (TPB) sites where electrons from Ni, lattice oxygen from the YSZ electrolyte, and the reactants in the gas phase meet [5,12]. According to Fig. 4(a), the initial performance of the Ni-based SOFC was high due to the high electrical conductivity and excellent catalytic reforming activity of the Ni-based anode [4,7]. For example, the initial performance shows an open cell potential of 1.0 V and a current density of 100 mA cm^{-2} at a cell potential of 0.9 V. These values are comparable to the values found in the literature for Ni-based SOFCs operated under similar conditions to those used in this study [6, 36,37]. However, during normal SOFC operation, the liquid fuels are cracked into carbon fragments at or near the TPB sites. As the cell operation time increases, these carbon fragments start to deposit and aggregate to form a coke layer over the Ni surface [4,10–12]. As a direct result of coke formation, the performance of the Ni-based SOFC decreases very rapidly with time and completely deactivates within 5 h as shown in Fig. 4(a).

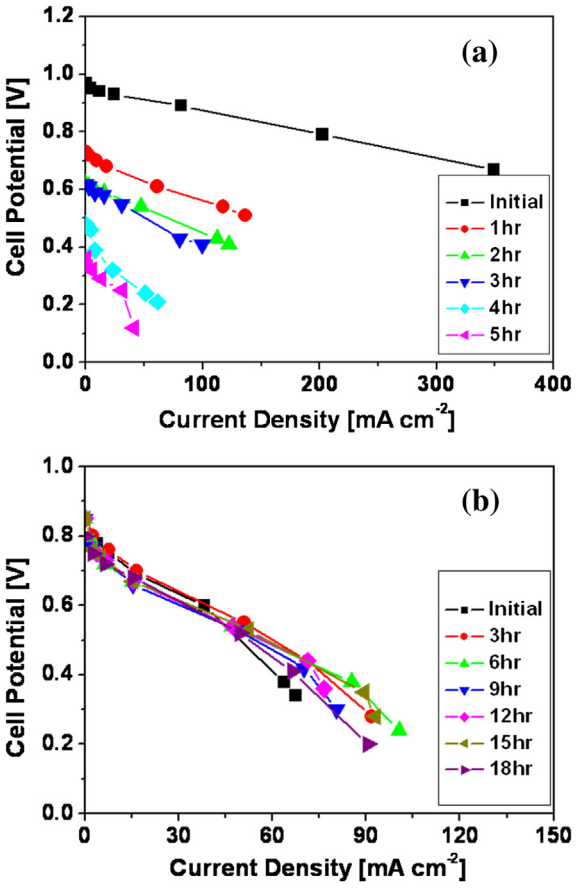

Fig. 4. Voltage–current density (*VI*) plots at different cell operation times for (a) the Ni-based and (b) MoO_2-based SOFC using *n*-dodecane, air and CO_2 mixtures as a fuel at 850 °C.

Fig. 4(b) shows *V–I* plot for a MoO_2-based SOFC under the same operating conditions used for the Ni-based SOFC. The *V–I* plots were taken every 3 h. Comparing Fig. 4(a) and (b), the initial performance of the MoO_2-based SOFC is lower than that of the Ni-based SOFC. The OCV is largely influenced by the partial pressure of each gas species that is in chemical equilibrium at the anode. The Ni-based and MoO_2-based anodes would give dissimilar gas compositions due to their different reforming activities toward *n*-dodecane. Thus, Ni-based and MoO_2-based SOFCs provide different initial OCV values. As the current increases, the initial *V–I* plot of the Ni-based SOFC linearly decreases following Ohm's Law. On the contrary, the initial *V–I* plot of the MoO_2-based SOFC drops more rapidly as the current increases, which is a characteristic of mass transfer limited cell performance. A SEM image of the tested MoO_2-based anode shows a dense film on the surface (see Fig. 5), which could explain the rapid cell potential drop by limiting the transport of reactants to the electrode surface.

Unlike the initial performances, the MoO_2-based SOFCs show higher stability. For example, at a cell potential of 0.6 V, the current density of MoO_2-based SOFCs remained at ~50 mA cm^{-2} over 18 h. This unusually high stability in the presence of liquid fuels can be explained in terms of the high coking resistance of MoO_2. As reported previously, the ability of MoO_2 to readily transport bulk lattice oxygen to the catalyst surface allows it to oxidize the carbon fragments before they agglomerate to form coke [20–22].

Fig. 6(a) and (b) shows power density plots for Ni-based and MoO_2-based SOFCs at 850 °C, respectively. Similar to the V-I plots shown in Fig. 4(a) and (b), the power density of Ni-based SOFCs shows a rapid drop with time, while that of the MoO_2-based SOFCs

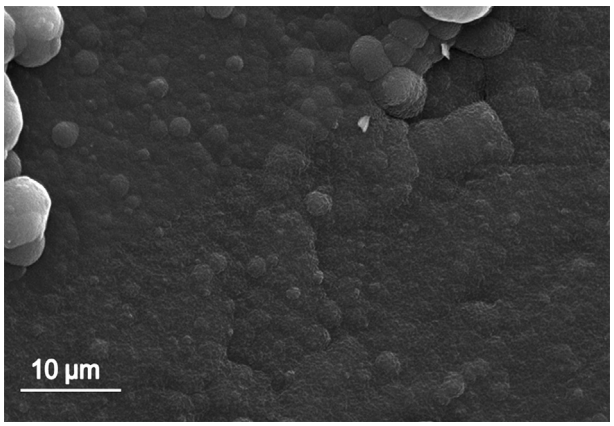

Fig. 5. SEM image of the MoO_2-based anode surface following 24-h operation.

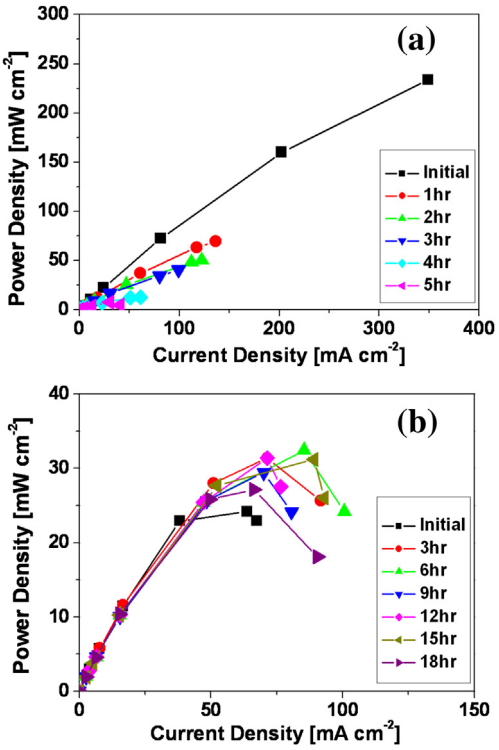

Fig. 6. Power density plots at different cell operation times for (a) the Ni-based and (b) MoO_2-based SOFC using *n*-dodecane, air and CO_2 mixtures as a fuel at 850 °C.

shows no apparent decrease as the cell operation time increases. If one carefully monitors the performance changes of the MoO_2-based SOFCs shown in Fig. 6(b), it can be noticed that the maximum power density increases from 25 mW cm^{-2} up to 34 mW cm^{-2} as the operation time increases for the first 6 h. This increase may be related to the formation of either a carbide phase (e.g., Mo_2C) and/or carbon nanotubes, which have a higher electrical conductivity than that of MoO_2 at 850 °C [38]. Even though these materials are not catalytically active for oxidizing *n*-dodecane, due to their high electrical conductivity their presence within the anode at a mild concentration level may reduce the electrical resistance of the anode. The evidence for the formation of both carbide and nanotubes are discussed in more detail later.

Fig. 7 shows the OCV of both Ni-based and MoO_2-based SOFCs as a function of operation time using *n*-dodecane. The initial OCV on the Ni-based SOFCs was 0.95 V, while that of the MoO_2-based cells was 0.85 V. The OCV of the Ni-based SOFCs declined very rapidly due to coke formation over the first 135 min of operation. However, the OCV temporarily increased at 135 min. It is speculated that this increase may be due to the formation of a thin film of carbon on the Ni-based anode [12,39]. This film can improve the electrical conductivity of the anode. After 135 min, the OCV of the Ni-based SOFC rapidly decreases again as carbon is continuously deposited over the anode.

Unlike the Ni-based SOFCs, the OCV of MoO_2-based SOFCs shows a stable value for the first 720 min. Its OCV oscillates between 0.87 and 0.76 V for the next 580 min, but it does not rapidly drop like the Ni-based SOFC. The change of the OCV values during the cell operation time between 720 and 1300 min can be explained in terms of carbide and/or carbon nanotube formation within the MoO_2-based anode. After 1300 min of operation time, the OCV value was stable again at 0.75 V.

Fig. 8 shows cross-sectional views of tested Ni-based and MoO_2-based anodes following their OCV measurements over 360 and

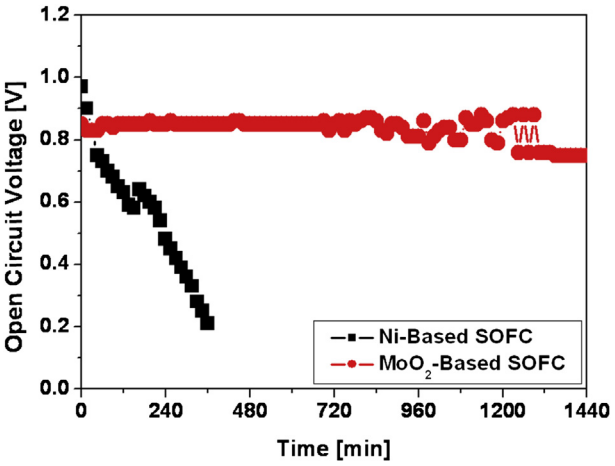

Fig. 7. Plot of open circuit voltage (OCV) as a function of operation time for the Ni-based and MoO_2-based SOFCs using *n*-dodecane, air and CO_2 mixtures as a fuel at 850 °C.

1440 min, respectively. The Ni-based anode exhibited substantial coke formation on the surface, which led to a rapid decline in cell performance. On the other hand, the MoO_2-based anode showed negligible coke formation, which explains its stable performance during continuous long-term testing.

In order to understand the degree of coke formation within the submicron layer of each tested anode, SEM-EDX analysis was

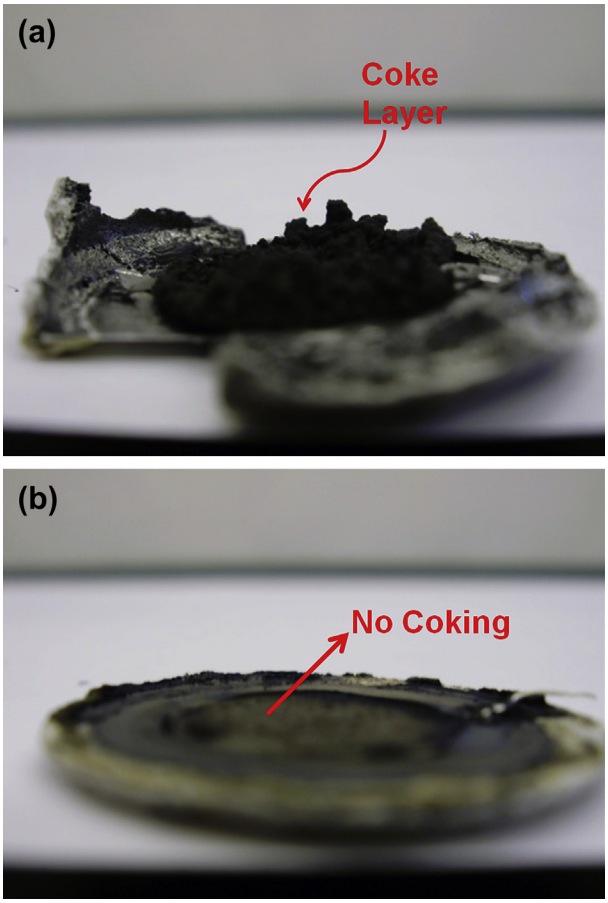

Fig. 8. Side views of (a) tested Ni-based and (b) tested MoO_2-based anodes obtained from long-term stability test using *n*-dodecane, air and CO_2 mixtures as a fuel at 850 °C.

performed. To do so, the thick carbon layer formed over the tested Ni-based anode was first removed followed by application of a thin sputtered gold layer to avoid charging under the electron beam. Fig. 9(a) shows a typical EDX spectrum observed from multiple point analyses. According to Fig. 9(a), the tested Ni-based anode contains 96.3 atomic % C. Based on XRD measurement of the tested Ni-based anode (data not shown) there is no indication of Ni-carbide formation. Thus, the excessive amount of carbon shown in the EDX data must come from coke deposited over the Ni-based anode. It is speculated that the tested Ni-based anode is covered with an amorphous coke layer because (1) XRD analysis showed no diffraction peaks for graphitic carbon and (2) the samples showed excessive charging without the sputtered gold layer.

Fig. 9(b) shows the EDX spectrum observed from multiple point analyses of the tested MoO_2-based anode. According to Fig. 9(b), the tested MoO_2-based anode contains mainly Mo and O with a small amount of C (6.7 atomic %). XRD analysis of the tested MoO_2-based anode was also performed (data not shown), and indicates the presence of both MoO_2 and Mo_2C phases. Thus, some of the MoO_2 was transformed to Mo_2C during cell operation.

It is well known that MoO_2 can capture elementary carbon or carbon fragments under highly reducing conditions and use them as a carbon source to transform the dioxide phase into the carbide phase [20,21]. In other words, MoO_2 can act as a solid phase carbon buffer to "absorb" excess amounts of surface carbon. Because of the metallic-like property of MoO_2, it can actively break down the long carbon chain fuel molecules into small carbon fragments. If the necessary amount of lattice oxygen is available at the fuel activation site, then these carbon fragments would be further oxidized into carbon oxides. However, if there is insufficient lattice oxygen available at the active site, these carbons can diffuse into the MoO_2 lattice structure rather than agglomerating to form coke. Since we used very reducing operating conditions for the anode, it seems that the initial MoO_2-based anode went through the phase transformation to form the Mo_2C phase during continuous long-term testing.

To regenerate the MoO_2 phase, one simply needs to feed steam to the anode. The steam can oxidize the Mo_2C into the MoO_2 phase without fully oxidizing it into the inactive MoO_3 phase at 850 °C [40]. In a very few isolated regions of the tested MoO_2-based anode, carbon nanotubes were found by SEM as shown in Fig. 10. According to the literature, both molybdenum [41–43] and Mo_2C [44,45] have been used for carbon nanotube synthesis.

In addition to using *n*-dodecane, biodiesel was used for cell operation to evaluate the fuel flexibility of MoO_2-based anodes. Fig. 11 shows *V*–*I* and power density plots at 850 °C. According to Fig. 11, the initial OCV is 0.92 V, which declines to 0.75 V within the first 4 h. However, the OCV increases back to 0.8 V over the following 1 h to remain stable until the end of the test period. Both the current density and maximum power density outputs follow a similar trend as the OCV. For example, the initial maximum power density is 45 mW cm^{-2}, which decreases to 35 mW cm^{-2} during the first 3 h. However, the value gradually increases back to 45 mW cm^{-2} over the next 1 h.

Shiratori et al. operated a SOFC by directly feeding three different biodiesels mixed with steam at 800 °C [46]. These biodiesels are synthesized by processing refined palm, jatropha, and soybean oils. The refined palm biodiesel generated the highest performance at 400 mW cm^{-2}. They also showed that the cell performance is greatly affected by the composition of the biodiesel. The chemical composition of biodiesel can vary over a wide range depending on what biomass was used as the precursor. For our study, we used canola biodiesel, which has a very different composition compared to the refined palm biodiesel. Since we directly fed canola biodiesel into the MoO_2-based SOFC, it is difficult to make a direct comparison of our cell performance to that of other groups who used biodiesels synthesized from different biomasses. Nevertheless, the results demonstrate that MoO_2-based anodes enable fuel flexibility because they can operate with both long-chain hydrocarbons such as *n*-dodecane and the oxygenated hydrocarbons present in biodiesel.

As discussed earlier, the MoO_2-based anode forms a dense film on the surface during its operation, which leads to its mass transfer limited low initial performance. To improve its initial performance

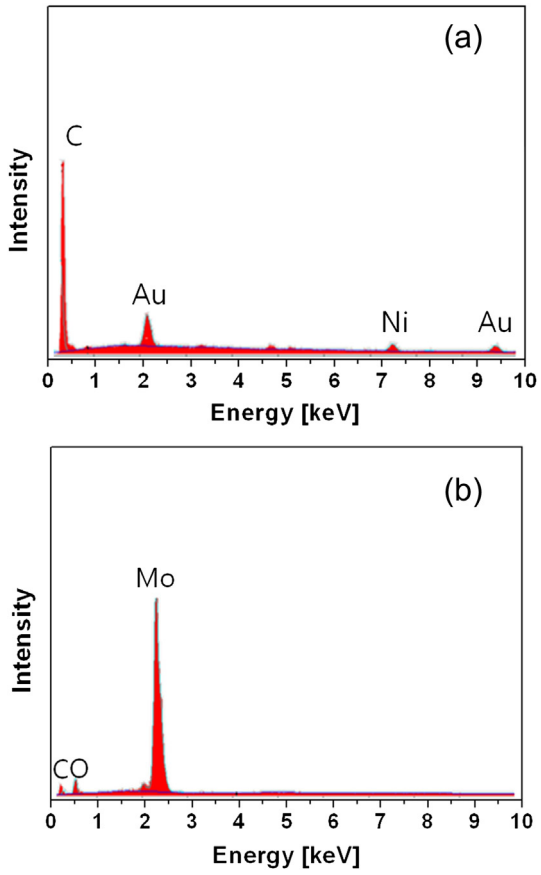

Fig. 9. EDX analysis of (a) tested Ni-based and (b) tested MoO_2-based anodes obtained from long-term stability test using *n*-dodecane, air and CO_2 mixtures as a fuel at 850 °C.

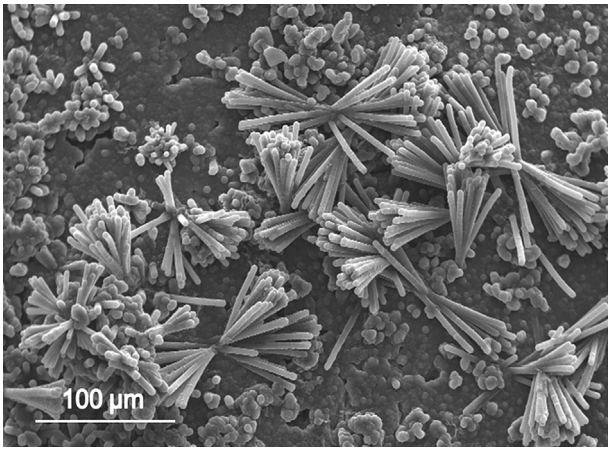

Fig. 10. SEM image of carbon nanotubes found in very limited spots of the tested MoO_2-based anode surface.

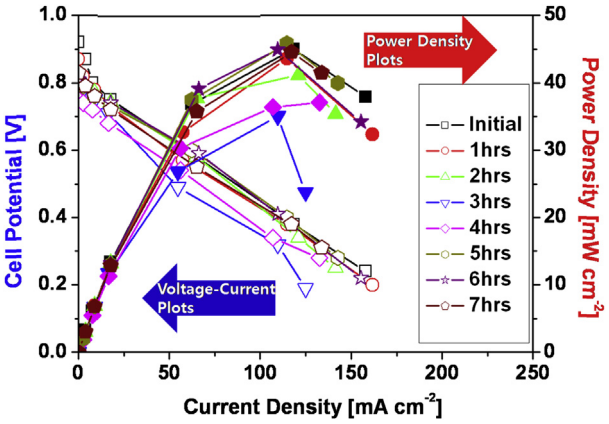

Fig. 11. Cell potential and power density vs. current density for MoO_2 anode using biodiesel, air and CO_2 mixtures as fuel at 850 °C every hour.

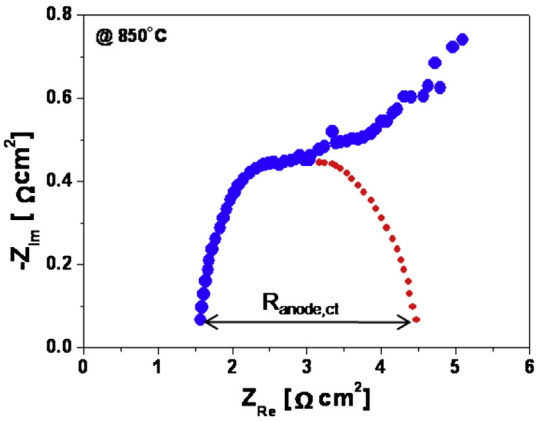

Fig. 13. Electrochemical impedance spectra under an open circuit voltage (OCV) condition of MoO_2-based SOFC using *n*-dodecane, air and CO_2 mixtures as fuel at 850 °C.

by increasing the film porosity, the concentration of PVA (i.e., pore former) was increased by a factor of 12 wt.% in the catalyst ink during the MoO_2-based anode preparation step. As shown in Fig. 12(a), the initial *V–I* plots of the MoO_2-based SOFC with the two different PVA concentrations were measured at 850 °C. The same *n*-dodecane fuel mixture was used as described in the experimental section. Compared to the MoO_2-based SOFC with the low PVA content, the *V–I* plot of the MoO_2-based SOFC with the high PVA content extends further out toward the higher current density output and shows a significantly improved power density output with a maximum power density of 2500 mW cm^{-2} (the power density plots are not shown). The fuel cells were continuously operated over 24 h at 850 °C under the OCV condition. At the end of 24 h test, we obtained *V–I* plots and examined the surface morphologies using SEM. According to Fig. 12(a), the cell performance decreased by a small percentage over 24 h, but it is important to point out that the MoO_2-based SOFC with the high PVA content still maintained the much higher cell performance than that of the cell with the low PVA content. As seen in Fig. 12(b) left and right, the MoO_2-based anode with the high PVA content following the 24 h

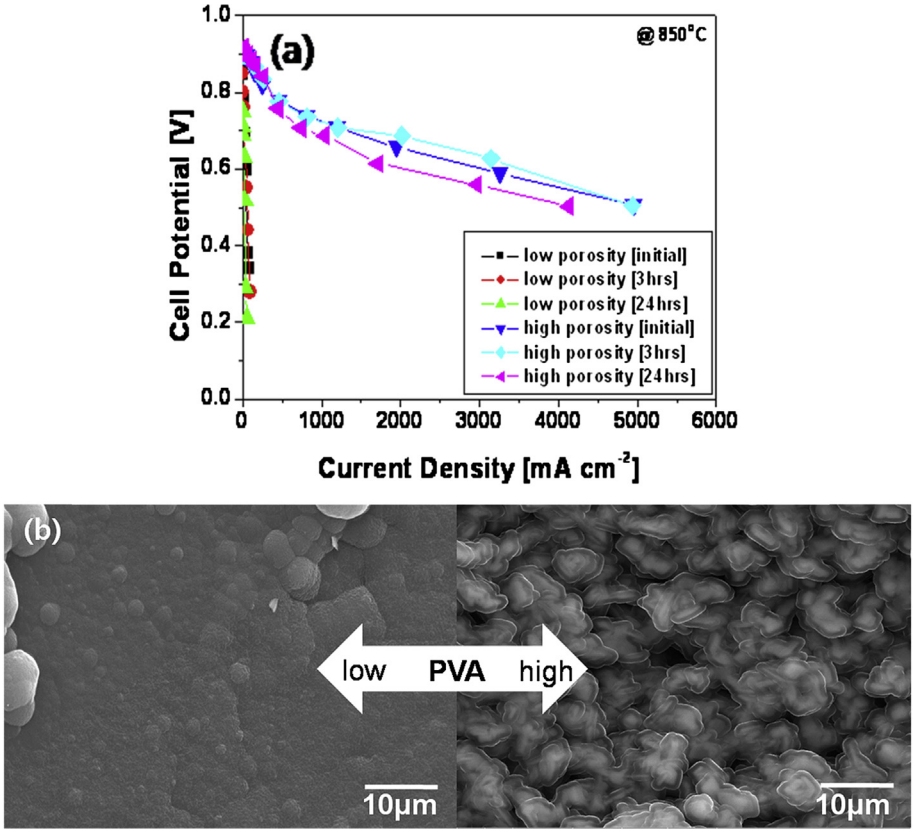

Fig. 12. (a) Cell potential vs. current density plots for the MoO_2-based anode with either a low or a high porosity using *n*-dodecane, air and CO_2 mixtures as fuel at 850 °C; (b) SEM images of the MoO_2-based anode with either a low porosity (left side) or a high porosity (right side) following the 24 h cell operation. The porosity of the MoO_2-based anode was controlled by the PVA (i.e. binder/pore former) content used during its preparation step.

test showed a much improved film porosity compared to that of the MoO_2-based anode with the low PVA content. In addition to the improved porosity, the MoO_2-based anode with the high PVA content maintained an excellent physical interconnection for proper charge and ion transports.

We believe that this unique surface morphology of the MoO_2-based anode with the high PVA content led to the increase of its initial performance as shown in Fig. 12(a). Currently, we are further optimizing the morphology of the MoO_2-based anode by changing the type and concentration of the pore former. Detailed characterization and optimization studies will be reported in a future paper. Fig. 13 shows the electrochemical impedance spectrum (EIS) of the MoO_2-based SOFC with the high PVA concentration after 3 h test at the OCV condition and a temperature of 850 °C. During the EIS measurement, the impedance of the MoO_2-based SOFC is obtained over a desired frequency range between 0.05 Hz–50 kHz. The diameter of the semi-circle of the impedance spectrum can be measured by extrapolating its last point in the low frequency region to the *x*-axis. The diameter of the semi-circle in Fig. 13 is referred to as the charge transfer resistance, R_{ct}, while the intersection point on the *x*-axis in the high frequency region is referred to as the electrolyte resistance, R_{ele}. The charge transfer resistance of LSM cathode with air at 850 °C is in the order of 0.1 Ω cm^2 [4]. Thus, we can assume that the R_{ct} value in Fig. 13 is equivalent to the charge transfer resistance of the MoO_2-based anode ($R_{anode,ct}$) with the *n*-dodecane fuel mixture. Based on the impedance spectrum, the $R_{anode,ct}$ is estimated to be about 3 Ω cm^2. This $R_{anode,ct}$ value is about one order of magnitude greater than that of the typical Ni-based SOFC using pure H_2 [4], but comparable to the Ni-based SOFC using *n*-dodecane [46].

4. Conclusions

This work investigated the performance of direct liquid fuel SOFCs using MoO_2-based anodes. The MoO_2-based anodes were found to be highly coke resistant when *n*-dodecane was used as a fuel and they exhibited significantly improved long-term stability when compared to Ni-based anodes. The MoO_2-based anodes also showed potential for fuel flexibility by directly operating with synthetic biodiesel formulated for airplane applications. Additionally, the initial performance of our MoO_2-based SOFC was improved up to 2500 mW cm^{-2} at 850 °C using *n*-dodecane as the fuel by optimizing the porosity of the MoO_2-based anode.

Acknowledgments

This work was supported financially by the National Science Foundation GOALI Program (Grant No. CBET-1034308) and by Boeing Commercial Airplanes.

References

[1] J. Larmine, A. Dicks, Fuel Cell Systems Explained, John Wiley & Sons Ltd., West Sussex, England, 2003.
[2] The American Ceramic Society, Process in Solid Oxide Fuel Cells, John Wiley & Sons, Inc., Hoboken, New Jersey, 2006.
[3] T. Ishihara, Perovskite Oxide for Solid Oxide Fuel Cells, Springer, New York, 2009.
[4] J.W. Fergus, R. Hui, X. Li, D.P. Wilkinson, J. Zhang, Solid Oxide Fuel Cells: Materials Properties and Performance, CRC Press Taylor & Francis Group, New York, 2009.
[5] M. Cimenti, J.M. Hill, Energies 2 (2009) 377–410.
[6] H. Kishimoto, Y. Xiong, K. Yamaji, T. Horia, N. Sakai, M.E. Brito, H. Yokokawa, ESC Transactions 7 (2007) 1669–1674.
[7] J.S. O'Brein, J.B. Giorgi, ESC Transactions 28 (2010) 221–231.
[8] K. Kendall, M. Slinn, J. Preece, Journal of Power Sources 157 (2006) 750–753.
[9] Z.F. Zhou, R. Kumar, S.T. Thakur, L.R. Rudnick, H. Schobert, S.N. Lvov, Journal of Power Sources 171 (2007) 856–860.
[10] A. Takeuchi, H. Wise, Journal of Physical Chemistry 87 (1983) 5372–5376.
[11] J. Hoh, Y. Yoo, J. Park, H.C. Lim, Solid State Ionics 149 (2002) 157–166.
[12] R.J. Gorte, J.M. Vohs, Journal of Catalysis 216 (2003) 477–486.
[13] H. Kim, S. Park, J.M. Vohs, R.J. Gorte, Journal of the Electrochemical Society 148 (2001) A693–A695.
[14] T. Kim, K. Ahn, J.M. Vohs, R.J. Gorte, Journal of Power Sources 164 (2007) 42–48.
[15] M.D. Gross, J.M. Vohs, R.J. Gorte, Journal of Materials Chemistry 17 (2007) 3071–3077.
[16] J.M. Vohs, R.J. Gorte, Advanced Materials 21 (2009) 943–956.
[17] V. Bhosle, A. Tiwari, J. Narayan, Journal of Applied Physics 97 (2005) 083539–083544.
[18] O. Marin-Flores, L. Scudiero, S. Ha, Surface Science 603 (2009) 2327–2332.
[19] M. Bengisu, Engineering Ceramics, Springer, Heidelberg, New York, 2001, ISBN 3-540-67687-2.
[20] O. Marin-Flores, T. Turba, C. Ellefson, K. Wang, J. Breit, J. Ahn, M.G. Norton, S. Ha, Applied Catalysis B: Environmental 98 (2010) 186–192.
[21] O. Marin-Flores, S. Ha, Applied Catalysis A: General 352 (2009) 124–132.
[22] O. Marin-Flores, T. Turba, C. Ellefson, J. Breit, M.G. Norton, S. Ha, Applied Catalysis A: General 381 (2010) 18–25.
[23] O. Marin-Flores, T. Turba, C. Ellefson, L. Scudiero, J. Breit, M.G. Norton, S. Ha, Applied Catalysis B: Environmental 105 (2011) 61–68.
[24] V. Vorontsov, W. An, J.L. Luo, A.R. Sanger, K.T. Chuang, Journal of Power Source 179 (2008) 9–16.
[25] Y. Huang, R.I. Dass, Z. Xing, J.B. Goodenough, Science 312 (2006) 254.
[26] I. Baldychev, A. Javadekar, D.J. Buttrey, J.M. Vohs, R.J. Gorte, Applied Catalysis A: General 394 (2011) 287–293.
[27] A. Aguadero, M.J. Martinez-Lope, V. Pomjakushin, J.A. Alonso, European Journal of Chemistry (2011) 3226–3231.
[28] C.A. Ellefson, O. Marin-Flores, S. Ha, M.G. Norton, Journal of Materials Science 47 (2012) 2057–2071.
[29] D. Marinha, C. Rossignol, E. Djurado, Journal of Solid State Chemistry 182 (2009) 1742–1748.
[30] C.H. Chen, M.H. Emond, E.M. Kelder, B. Meester, J. Schoonman, Journal of Aerosol Science 30 (1999) 959–967.
[31] I. Taniguchi, R.C. van Landschoot, J. Schoonman, Solid State Ionics 160 (2003) 271–279.
[32] R. Neagu, E. Djurado, L. Ortega, T. Pagnier, Solid State Ionics 177 (2006) 1443–1449.
[33] M. Cloupeau, B. Prunet-Foch, Journal of Electrostatics 22 (1989) 135–159.
[34] B. Hwang, C. Chang, C. Hsu, C. Fu, Journal of Physics D: Applied Physics 40 (2007) 3448–3455.
[35] A. Princivalle, E. Djurado, Solid State Ionics 179 (2008) 1921–1928.
[36] H. Kishimoto, T. Horita, K. Yamaji, Y. Xiong, N. Sakai, M.E. Brito, H. Yokokawa, Journal of Electrochemical Society 152 (2005) A532–A538.
[37] H. Kishimoto, K. Yamaji, Y. Xiong, T. Horita, M.E. Brito, H. Yokokawa, ECS Transactions 17 (2009) 31–35.
[38] S.T. Aruna, M. Muthuraman, K.C. Patil, Solid State Ionics 111 (1998) 45–51.
[39] C.B. Carter, M.G. Norton, Ceramic Materials: Science and Engineering, Springer, New York, 2007, ISBN 0-387-46270-8.
[40] O. Marin-Flores, S. Ha, Catalysis Today 136 (2008) 235–242.
[41] A. Dhir, K. Kendall, Journal of Power Sources 181 (2008) 297–303.
[42] K.B.K. Teo, C. Singh, M. Chhowalla, W.I. Milne, Encyclopedia of Nanoscience and Nanotechnology X, 2003, pp. 1–22.
[43] H. Dai, A.G. Rinzler, P. Nikolaev, A. Thess, D.T. Colbert, R.E. Smalley, Chemical Physics Letters 260 (1996) 471–475.
[44] J.H. Hafner, M.J. Bronikowski, B.R. Azamian, P. Nikolaev, A.G. Rinzler, D.T. Colbert, K.A. Smith, R.E. Smalley, Chemical Physics Letters 296 (1998) 195–202.
[45] W.P. Leroy, C. Detanernier, R.L. Meirhaeghe, A.J. Kellock, C. Lavoie, Journal of Applied Physics 99 (063704) (2006).
[46] Y. Shiratori, T.Q. Tran, Y. Takahashi, K. Sasaki, ESC Transactions 35 (2011) 2641–2651.